Available online at www.sciencedirect.com
SCIENCE DIRECT®
Tectonophysics 368 (2003) 51–69
TECTONOPHYSICS
www.elsevier.com/locate/tecto

2-D seismic trenching of colluvial wedges and faults

David Sheley, Travis Crosby, Min Zhou, Jamie Giacoma, Jianhua Yu, Ruiqing He, Gerard T. Schuster*

Geology and Geophysics Department, University of Utah, 135 S. 1460 E., Rm 713 Browning Building, Salt Lake City, UT 84112, USA

Received 13 September 2002; accepted 10 March 2003

Abstract

Images of the depth and shape of colluvial wedges by 3-D travel time tomography can be valuable in estimating the past history of ancient earthquakes and assessing the earthquake hazard of a fault. Unfortunately, 3-D seismic surveys can be both costly and time consuming. In this paper, we report out first successful results of detecting the shapes and depths of colluvial wedges with 2-D travel time tomography. The locations of the colluvial wedges are along the Oquirrh fault and the Salt Lake City segment of the Wasatch fault. We also report that the tomogram from one of our 2-D surveys suggests the possibility of detecting multiple colluvial wedges at depth. Using both reflection and tomographic images at another site clearly reveals the presence of a known shallow fault and the contact between native soil and recent fill. Our results suggest the synergistic use of both seismic tomography and reflection imaging, we denote as seismic trenching, as a means of detecting shallow colluvial wedges and faults. Seismic trenching has the potential to significantly expand the lateral extent and depth of investigation of paleoseismology.

Keywords: Tomography; Colluvial wedge; Wasatch fault; Oquirrh fault; Seismic trenching; Migration

1. Introduction

Morey and Schuster (1999) showed that 3-D seismic tomography is capable of delineating the shape and depth of a colluvial wedge across a normal fault (see Fig. 1). They proposed that seismic trenching, i.e., 3-D tomography combined with 2-D reflection imaging (Stephenson et al., 1993), can inexpensively provide deeper and wider (albeit less resolved) images of fault systems than the standard excavation and logging of trenches across faults. The principle conjecture in their procedure is that colluvial wedges are characterized by detectably lower P-wave velocity than the surrounding alluvium. This conjecture was supported by data presented in Morey and Schuster (1999) and is further supported by new data presented in this paper. They also proposed that the recurrence intervals of ancient earthquakes could be determined by drilling through the identified wedge and using either a thermoluminescence or a radiocarbon dating technique to date the core samples. Thus, seismic imaging can add an extra dimension and a deeper perspective to the palaeoseismic information gained from a 2-D trench excavation. When trench excavation is impractical, seismic trenching might provide the only alternative.

Unfortunately, 3-D seismic experiments and the subsequent data processing are both costly and time consuming with current technology. For example, the 2-week 3-D experiment of Morey and Schuster (1999) recorded more than 110,000 seismic traces over a 10 ×

* Corresponding author. Tel.: +1-801-581-4373; fax: +1-801-581-7065.
E-mail address: schuster@mines.utah.edu (G.T. Schuster).

0040-1951/03/$ - see front matter © 2003 Elsevier Science B.V. All rights reserved.
doi:10.1016/S0040-1951(03)00150-1

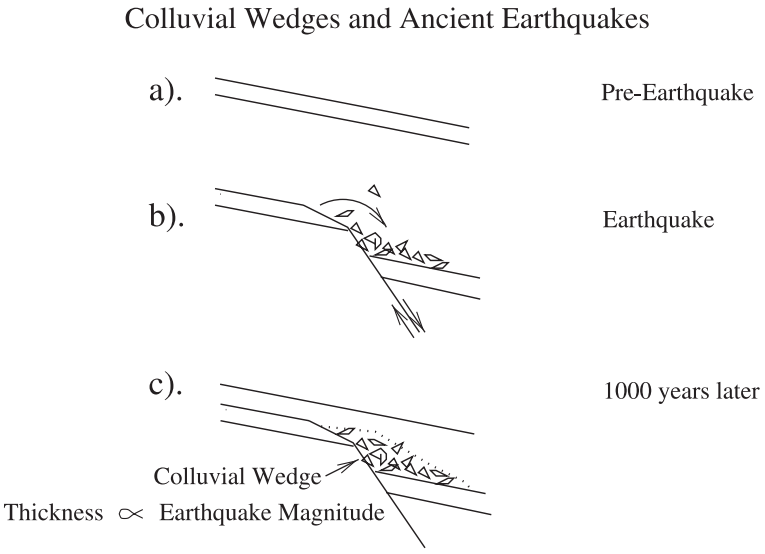

Fig. 1. Colluvial wedge (a) before, (b) during, and (c) after an earthquake rupture. The thickness of the colluvial wedge is proportional to the displacement along the fault or magnitude of the event. The thickness interval between adjacent colluvial wedges is proportional to the recurrence interval.

52 m patch of ground. In addition to requiring several hundred man-hours of labor, it required a roll-along box, a 60-channel recorder, a 48-channel recorder, and 300 geophone stations. Such equipment and manpower costs can discourage many engineering firms from pursuing 3-D experiments until the recording technology becomes more efficient and affordable. As an alternative, we show in this paper that 2-D seismic experiments can be inexpensively carried out and still yield travel time tomograms where the colluvial wedge is clearly delineated. In addition, the reflection images can also be used to delineate the fault geometries, which is very useful for earthquake hazard studies (McCalpin, 1996). A 2-D seismic trenching experiment across a fault can be carried out in about 6 h by a crew of two.

For this study, we collected seismic data at three sites along the Wasatch Fault Zone (WFZ) and one site on the northern part of the Oquirrh fault. The seismic survey along the northern part of the Oquirrh fault was adjacent to the Big Canyon trench site of Olig et al. (1996) and was coincident with the 3-D seismic survey of Morey and Schuster (1999). Two of the survey sites along the Wasatch Fault Zone were along the southern part of the Salt Lake City segment: Hidden Valley Park, UT where a previous study (Delta Geotech., 1994) excavated a trench, and the Megatrench site where McCalpin and associates excavated a trench in 1999 (McCalpin and Nelson, 2000). These data are processed to produce both tomograms and reflection sections that reveal 2-D images of possible colluvial wedges and the fault geometries over the study areas. The third survey along the WFZ took place on the football field at Judge High School, located near the northern part of the Salt Lake City segment.

Our work is presented in four parts: a summary of the background seismicity along the Wasatch Fault Zone, Utah, description of the tomography method and the data acquisition procedure, results of tomographic and reflection imaging, and a summary.

To view the color figures in this paper, see the online version to be found at doi:10.1016/S0040-1951(03)00150-1.

2. Background seismicity

2.1. Wasatch fault zone, Utah

The Wasatch fault, shown in Fig. 2, is a 370-km-long normal fault that has not had a historical surface-faulting earthquake. Historical seismicity (Smith and Arabasz, 1991) in adjacent parts of the Intermountain

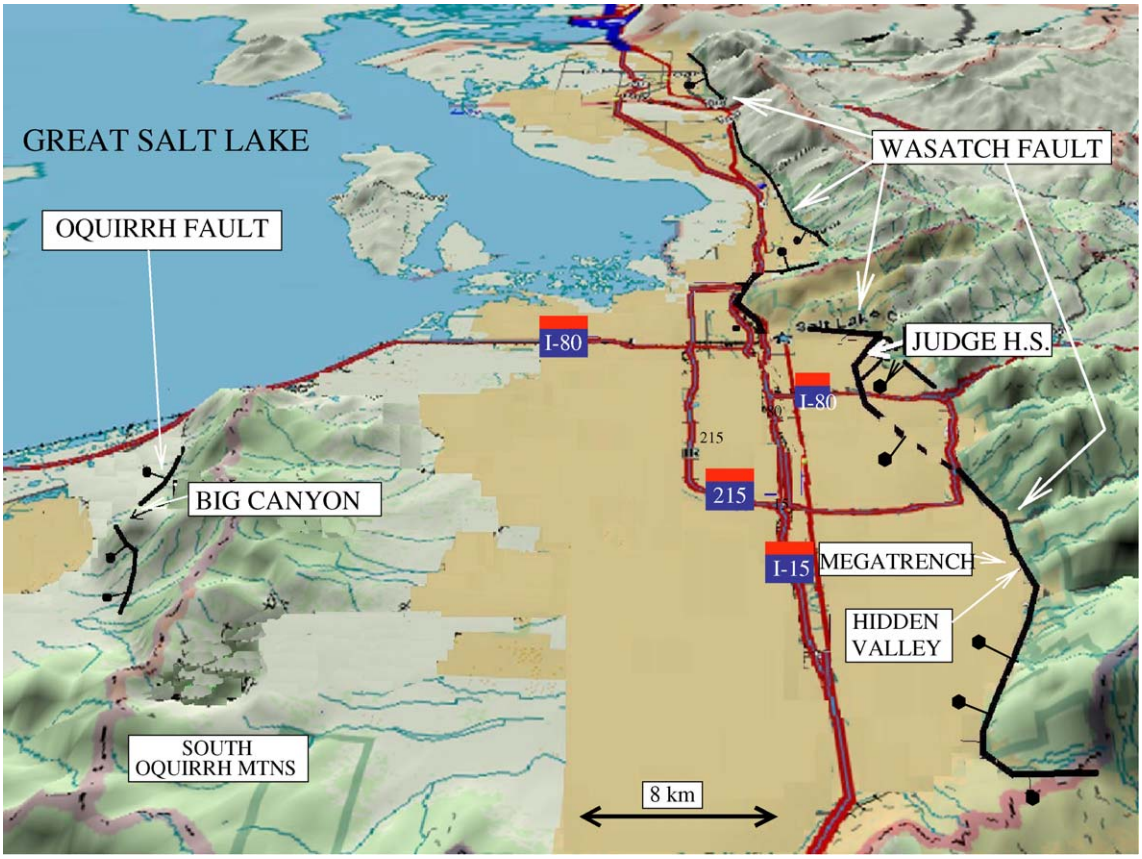

Fig. 2. Northward looking view of Salt Lake Valley with Wasatch and Oquirrh faults denoted by thick black lines. The four seismic survey sites are at Big Canyon (Olig et al., 1996), Hidden Valley Park (Delta Geotech., 1994), the Megatrench (McCalpin and Nelson, 2000), and the Judge High School football field.

Seismic Belt includes large magnitude earthquakes (M>6.5) in southern Idaho and northern Utah. Geologic and trench studies of the Wasatch fault suggest that the Wasatch fault is divided into at least eight segments, ranging in length from 35 to 65 km (Schwartz and Coppersmith, 1984). The Salt Lake City segment underlies Salt Lake Valley (Fig. 2) and has ruptured at least four times in the last 6000 years, generating earthquakes of Mw 6.9 or larger (Black et al., 1996). The average recurrence interval for surface faulting earthquakes in this segment is 1350 ± 200 years, with the most recent earthquake about 1300 (± 250) years ago (Black et al., 1996).

The combined average repeat time for large earthquakes (magnitude greater than 7) on any of the five central segments (Brigham City, Weber, Salt Lake City, Provo, and Nephi segments) of the Wasatch fault zone is 350 years. The average repeat time on any single segment ranges from about 1200 to 2600 years. The time since the last earthquakes on the five central segments ranges from 620 to 2120 years. Based on geologic studies and assuming that earthquakes are random, the probability of a large earthquake on the central segments of the Wasatch fault alone is 13% in 50 years and 25% in 100 years. On the Salt Lake City segment, the probability may be as high as 57% in 100 years (McCalpin and Nishenko, 1996).Thus, it is important that the data used in such statistical estimates are as reliable as possible, indicating the need for more trench studies.

2.2. Oquirrh fault zone, Utah

The Oquirrh Mountains are located in the eastern Great Basin directly west of Salt Lake City, UT, as

shown in Fig. 2. Active normal faults are located along the western side of the range (Gilluly, 1928).The northern fault zone near the Great Salt Lake is marked by a discontinuous series of Holocene-age scarps located at the base of a steep mountain front (Olig et al., 1996). Late Pleistocene shorelines of Lake Bonneville are cut into the mountain front well above the line of Holocene fault scarps, suggesting relatively rapid uplift of the mountain block relative to the basin floor during the late Quaternary. Different structural style and geomorphology suggest that the history of faulting, and the nature of seismic hazards, are significantly different between the northern and southern parts of the Oquirrh Mountains (e.g., Gilluly, 1928; Wu and Bruhn, 1994; Olig et al., 1996; Handwerger et al., 1999).

In the spring of 1996, researchers at the University of Utah conducted a 3-D seismic survey across the north Oquirrh fault, Utah (Morey, 1997; Morey and Schuster, 1999) at the Big Canyon trench site (Olig et al., 1996). This was followed by a long 2-D seismic traverse in 1997. The scientific objective was to use the resulting reflectivity and tomographic images to deduce the palaeoseismic history of this fault zone. This site was ideal for such a survey because it overlapped the study area of Olig et al. (1996) that trenched a colluvial wedge with a thickness of approximately 3 m along this part of the fault. This wedge was estimated to be the sediment signature of an ancient 7.0 moment magnitude earthquake that ruptured this fault more than a thousand years ago. Morey and Schuster (1999) presented accurate 3-D images of the Big Canyon wedge, and in this new paper, we present the tomographic images obtained from the 2-D data.

3. Methods

This section describes the refraction imaging methodology and the experimental procedures for imaging colluvial wedges. We also briefly describe the procedure for computing the stacked and migrated reflection sections.

3.1. Description of seismic experiment

The goal of the seismic experiments is to record 2-D seismic data with a fine enough geophone/source spacing and with a sufficiently high source frequency so that colluvial wedges buried to depths of about 10 m can be imaged with a spatial resolution of about 1 m. To achieve this goal, we employed a geophone and source spacing of either 0.5 or 0.66 m and a hammer source with a usable source frequency of more than 150 Hz. The source positions coincided with the geophone locations in order to use reciprocity (Lutter et al., 1990; Matheney et al., 1997; Morey and Schuster, 1999) as a means to identify inconsistent travel times. Table 1 summarizes the parameters for the field experiments.

Particle velocity geophones of either 40 or 48 Hz were planted along the surface perpendicular to the strike of the fault, so that (where practical) the midpoint of the survey line is over the presumed colluvial wedge. As an example, Fig. 3 shows a view of the Megatrench area and Fig. 4 depicts the 2-D seismic line straddling the nearby Wasatch fault.

3.2. Refraction tomography

Refraction tomography is a standard methodology for reconstructing the subsurface velocity distribution from first-arrival travel times (Nolet, 1987; Lutter et al., 1990; Aldridge and Oldenburg, 1993; Ammon and Vidale, 1993; Nemeth et al., 1997 and many others). Briefly, an initial velocity model is estimated from the $x-t$ slopes of the arrivals, the refraction rays are traced through this model to give calculated travel times, a misfit function is computed consisting of the sum of the squared travel time differences between the observed and computed travel times, and the model is adjusted until the misfit is minimized.

For the examples in this paper, we use the multigrid SIRT algorithm described in Morey and Schuster (1999) and Nemeth et al. (1997), which incorporates multigrid-like smoothing filters. The slowness field is assumed to be constant in each pixel. The iterations are

Table 1
Parameters for Megatrench (MT), Hidden Valley Park (HP), Oquirrh Big Canyon (BC) and Judge High School (JU) seismic surveys

Survey	Number of shots	Number of receivers/shot	Shot/receiver spacing (m)
Megatrench	168	168	0.5
Hidden Park	120	96	0.5
Big Canyon	384	96	0.5
Judge High School	240	120	0.66

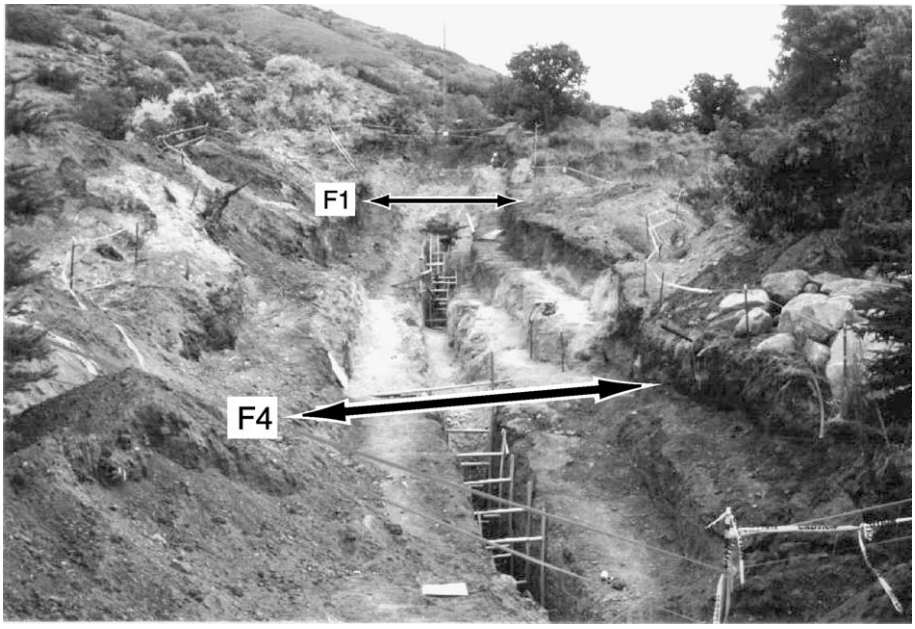

Fig. 3. Megatrench looking east. The approximate strikes of the F1 and F4 faults are denoted by arrows (photo from McCalpin and Nelson, 2000).

Fig. 4. Survey line and Megatrench line looking southeast; truck is near the midpoint of the line in Fig. 7 and the F1 and F4 fault locations (McCalpin and Nelson, 2000) are approximately denoted by the arrows.

stopped when the RMS travel time residual is less than the average travel time pick error. In all cases, the picking error was taken to be about 2 ms, which is about 1/6 of the dominant period of the first arrival. The velocities in the deeper unvisited pixels are assigned the same velocity as those from the nearest overlying pixel visited by a ray. This results in "striped" velocity contours in the deep unvisited regions, which are to be ignored in the interpretation (Morey, 1997).

3.2.1. Tomogram resolution

Using the empirical rule of thumb that the shot-receiver offset to refraction imaging depth ratio is 4:1, numerical experiments suggested that168 equal-spaced phones over an aperture of 84 m can image colluvial wedges to a depth of 10 m or more. This claim is supported by an empirical checkerboard test where rays are traced through a velocity gradient model and surface elevation similar to that found in the Megatrench survey. The checkerboard variation in velocity (top model in Fig. 5) is superimposed on a velocity gradient model and synthetic travel times from 168 shot gathers (168 traces/shot gather) are generated by ray tracing. The source and receiver spacings are identical to the actual Megatrench survey (see Table 1). The synthetic travel times are inverted by the tomography algorithm

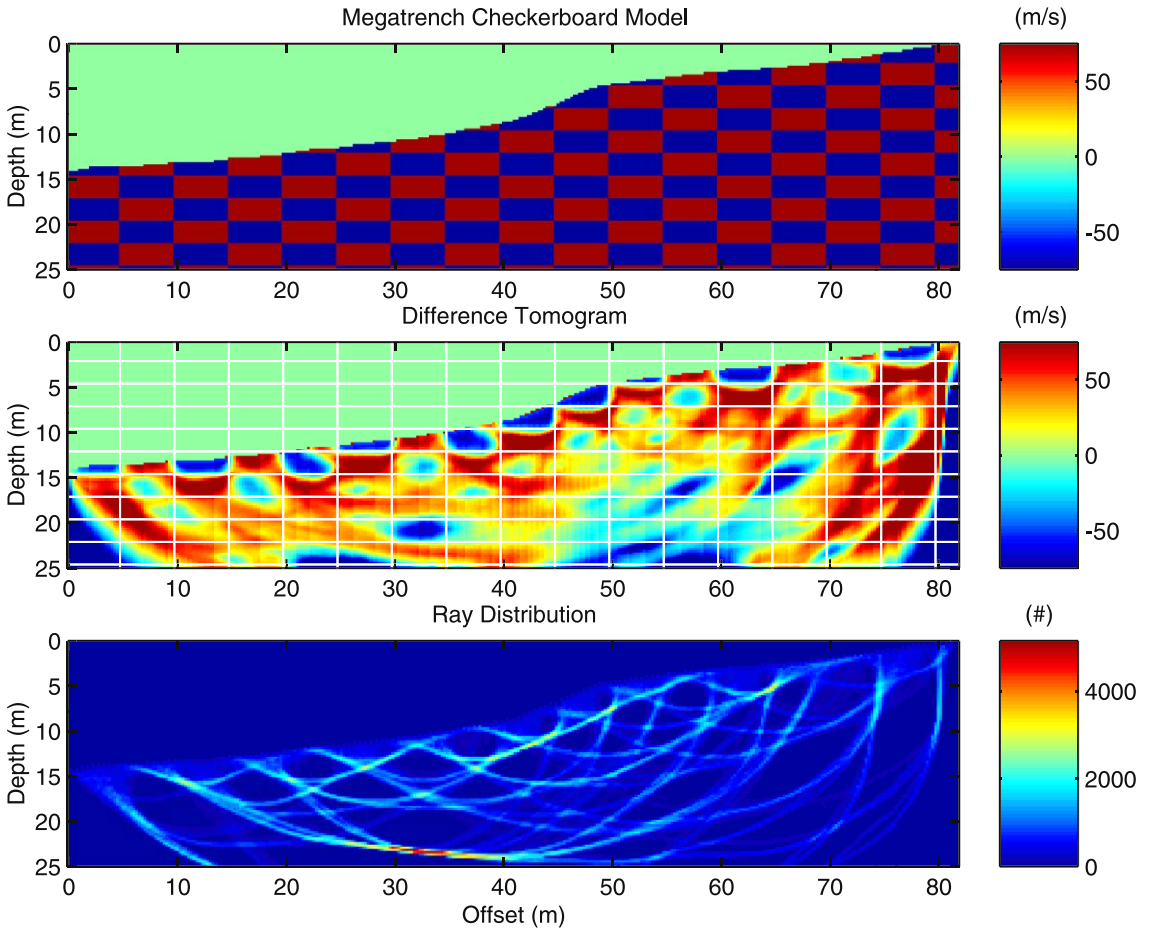

Fig. 5. (Top) Checkerboard model where the rectangles are 5 m by 2.5 m with a 150 m/s velocity contrast. The gradient velocity is not shown, but linearly trends from 200 m/s at the surface to the value 1300 m/s at 40 m depth. (Middle) Difference tomogram with 0.9 RMS travel time residual inverted from 168∗168 = 28,224 synthetic travel times (shooting geometry same as Megatrench in Table 1).The background gradient velocity has been subtracted from the final tomogram to give the above difference tomogram. (Bottom) Raypath density image.

to give the resulting tomogram shown in Fig. 5. It can be seen that the 5 m by 2.5 m rectangles are practically resolved to a depth of about 12 m below the surface for the central part of the model. As expected, the reconstruction becomes more smeared with increasing depth, but it was surprising that the ratio of source–receiver offset to accurate imaging depth was nearly 7–1! Note the surface topography imposes an acquisition footprint on the tomogram.

Spatial resolution is not only a function of source–receiver geometry, but it is also limited by the frequency content of the first-arrivals (Williamson and Worthington, 1993; Schuster, 1996; Sheng and Schuster, 2000). The first arrivals in the Megatrench shot gathers (e.g., Fig. 6) are characterized by signal frequencies (e.g., Fig. 7) in excess of 130 Hz for offsets out to 20 m. The corresponding wavelength is approximately 3.0 m, assuming a P-velocity of 400 m/s for shallow sediments. Taking into account Fresnel zone limits Δx (Schuster, 1996), a spatial resolution of little more than 5.5 m can be expected according to the formula $\Delta x = \sqrt{\lambda L/2} = \sqrt{3 \cdot 20/2} = 5.5\text{m}$. Here, L is the ray path length between the source and receiver.

The above theoretical resolution limit appears to be somewhat too pessimistic according to the synthetic tests of Mattson (2003). Mattson inverted travel times picked from synthetic data generated by a finite-difference solution to the acoustic wave equation for typical colluvial wedge models. In her tests, the shooting geometry was similar to that for our field tests, the wedge dimensions ranged between 4 and 12 m and wedges were buried at depths between 2 and 10

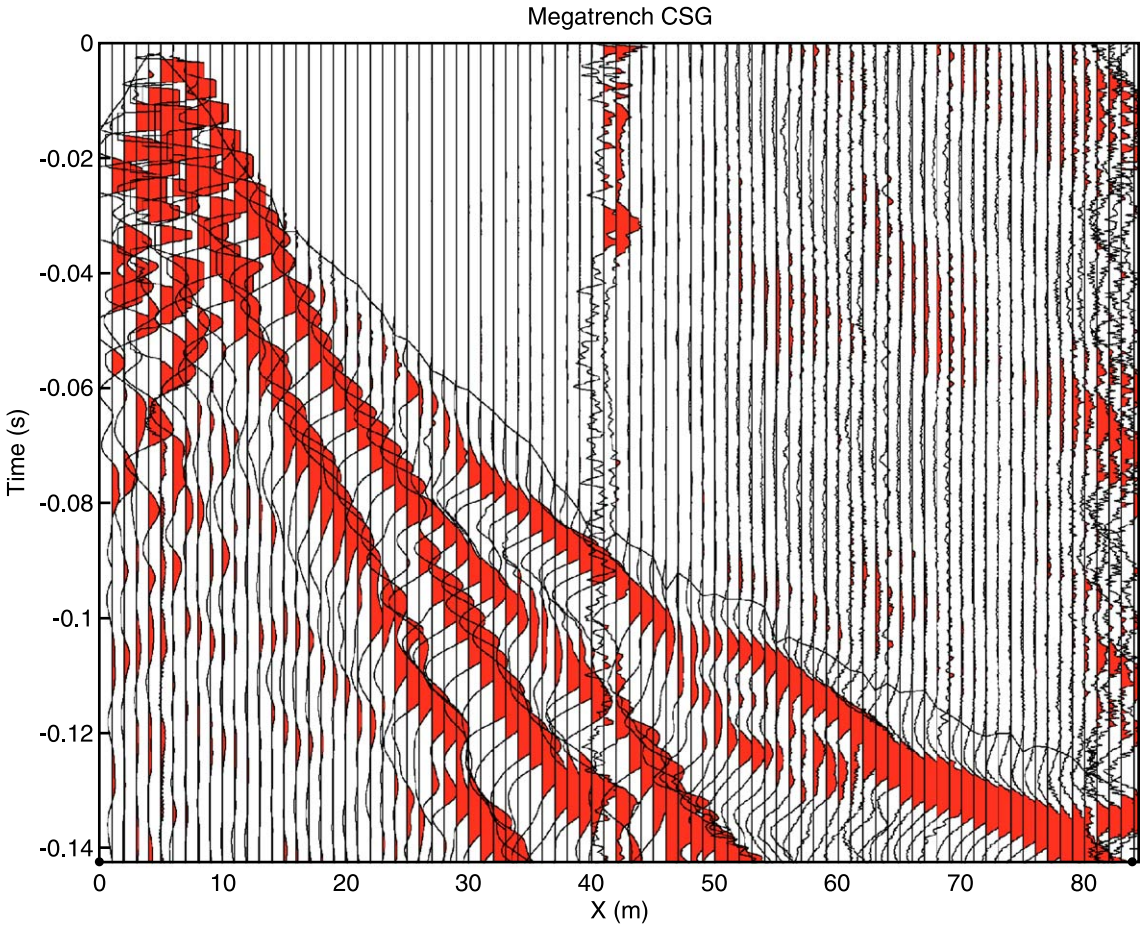

Fig. 6. A Megatrench shot gather with picked travel times denoted by the solid dark line. There are 168 traces per shot gather.

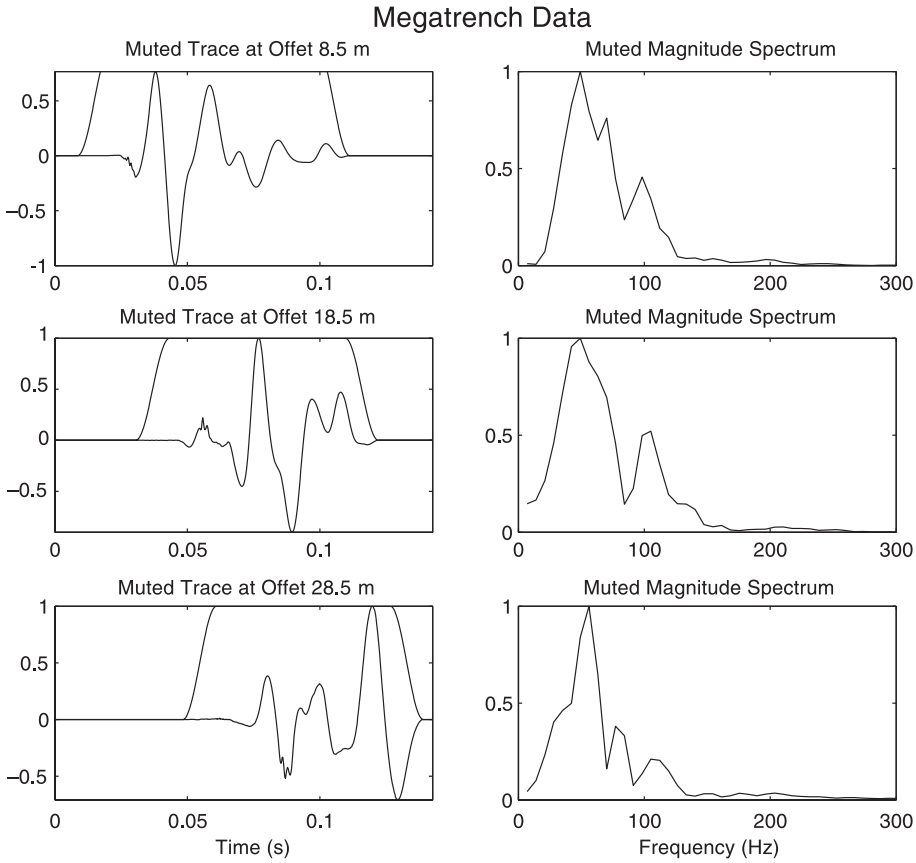

Fig. 7. Traces from Megatrench shot gather and associated spectrums. Traces were windowed about the first arrival using a squared cosine taper denoted by a solid line on each trace.

m, and the Ricker source frequency peaked at less than 80 Hz. Inverting the travel times showed an image (albeit smeared) of each low-velocity zone (LVZ) whose position coincided with the buried wedges. The LVZ anomalies were defined to be wedge-like low-velocity bodies surrounded by higher velocity material. Her result is consistent with the field data results of Morey and Schuster (1999) who inverted 100 Hz travel time data to unambiguously image wedges with a height of 3 m and a width of 6 m.

3.3. Description of reflection processing

Reflection processing typically consisted of the following steps: muting of coherent noise, band-pass filtering, FK filtering to suppress surface waves, velocity analysis, elevation statics, velocity analysis, residual statics, and a form of spectral whitening such as spectral balancing or predictive deconvolution. In the case of the Oquirrh data, trim statics (Yilmaz, 1987) was found to be effective in aligning the moveout corrected events so they stacked coherently. Typically, a careful NMO velocity analysis proved more effective in coherently stacking reflections than stacking with the tomogram velocity. Poststack migration provided some minor enhancements, but prestack migration failed to significantly enhance the sections. This is probably because we did not devote considerable efforts to maximize its inherent strengths. Although the tomograms gave excellent velocity control, the biggest obstacles to coherent stacking of reflections were the presence of coherent noise (probably due to near-surface scattering) and statics errors due to near-surface velocity anomalies.

Table 2
Inversion parameters for Megatrench, Hidden Park, Big Canyon Oquirrh and Judge tomograms

Survey	Grid size (m)	Grid dim of model	Number of travel times	Number of iterations	Final smoothing filter x by z (m)	RMS residual (ms)
MT	0.25	328 × 161	26 910/28 224	23	2.0 × 1.0	1.6
HP	0.15	401 × 201	8725/12 503	24	0.6 × 0.3	2.3
BC	0.15	1283 × 401	30 313/36 864	30	1.2 × 0.6	1.9
JU	0.15	480 × 80	≈13 000/14 400	18	1.5 × 0.8	2.3

The number of travel times that passed the reciprocity check is shown as the smallest number in the "Number of travel times" column, while the highest number represents the total number of picked travel times. Picking errors were estimated to be about 2 ms for all data sets.

In most of the reflection processing, shell-script commands using the SU processing package were used to process the data. However, the best results were obtained with the Judge data using commercial processing software with a graphical interactive capability. The convenience of graphical interactivity allowed us to easily test many "what-if" scenarios in real time compared to the more limited shell-script processing.

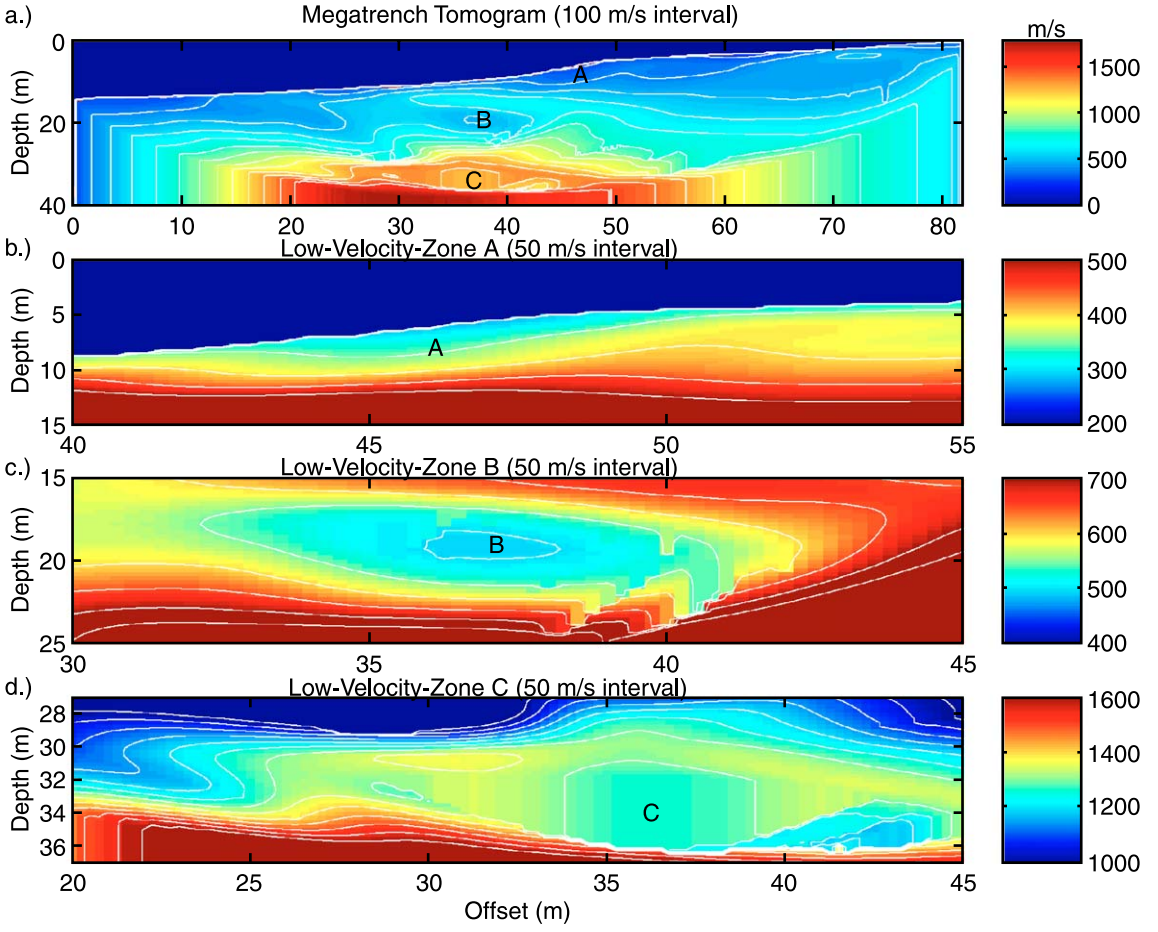

Fig. 8. Tomogram in (a). inverted from the Megatrench traveltime data. The (b) (c) and (d) tomograms are expanded views of low-velocity zones labeled by A, B, and C. Vertical stripes denote region where rays do not penetrate and are deliberately created by the inversion code to denote such areas.

4. Imaging results

The seismic data and tomograms from four seismic experiments are now presented. In each experiment, the goal was to image the shape and locations of colluvial wedges or faults over four different locations:

1. Megatrench site along the southern part of the Salt Lake segment of the Wasatch fault,
2. Hidden Valley Park, which is a part of the Wasatch fault located in the southern part of the Salt Lake Valley and is about six blocks from the South Fork Dry Creek trench,
3. Northern part of the Oquirrh fault (Morey and Schuster, 1999) at the Big Canyon trench site,
4. Judge High School along the northern part of the Salt Lake segment.

In the first three surveys, the station and source intervals were 0.5 m, and the source locations were coincident with the geophone locations. The Judge High School survey used a 0.66-m station interval.

4.1. Megatrench results

The Wasatch fault "Megatrench" was excavated by McCalpin and associates (McCalpin and Nelson,

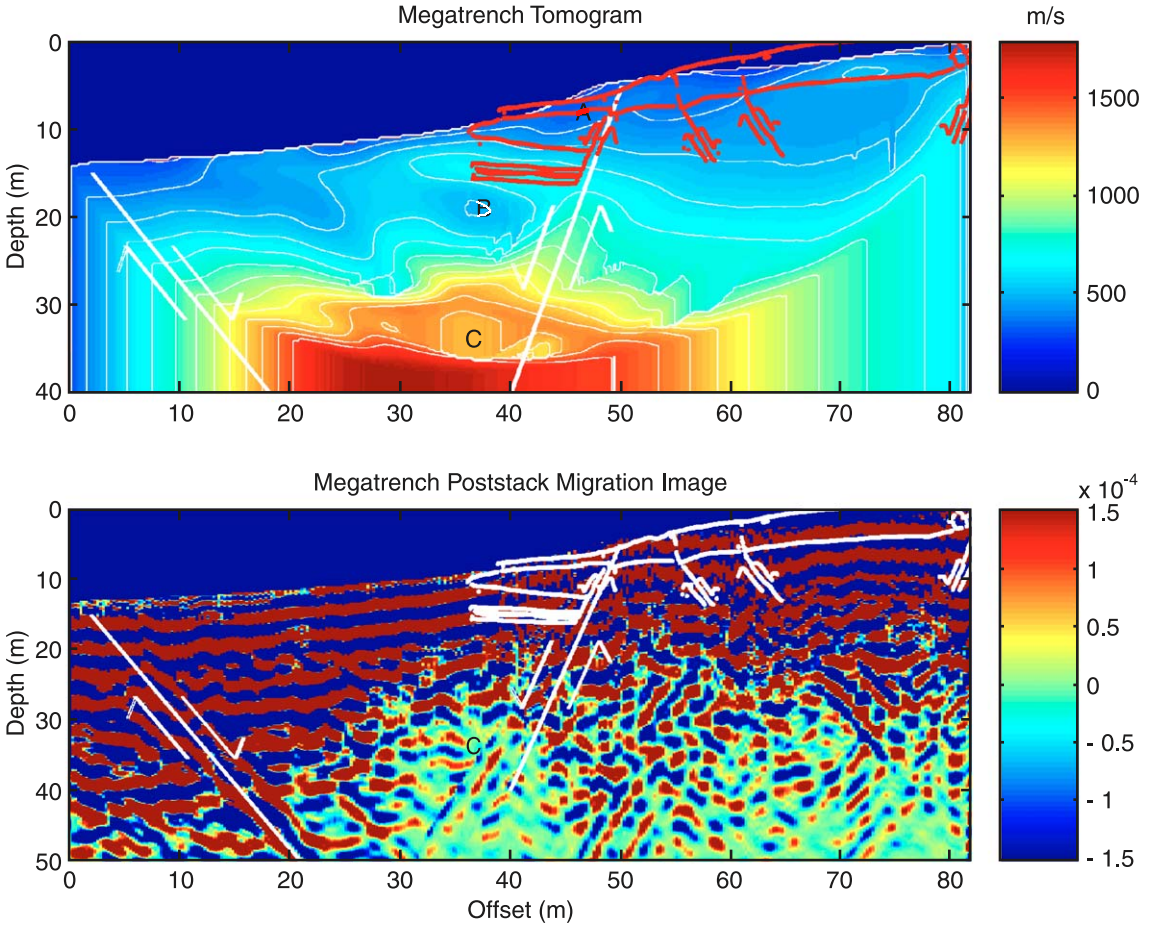

Fig. 9. (Top) Megatrench tomograms and (bottom) poststack migration images with interpreted faults (white lines) overlain a red drawing of the F4 colluvial wedge redrawn from McCalpin and Nelson's trench log. The ground surface of McCalpin's trench log does not exactly match the ground surface from the seismic profile because the survey line was about 20 m to the north and subparallel to the trench.

2000) in the fall of 1999 across an 18-m-high double-scarp of the Salt Lake City segment of the Wasatch fault zone (WFZ), 1 km north of the mouth of Little Cottonwood Creek. Fig. 3 shows a view of the trench looking east, where McCalpin and Nelson (2000) state the following:

> The trench and accompanying auger hole exposed 26 m of vertical section, roughly four times that of the typical trench on the WFZ. Each of the two fault scarps (upper fault labeled F1 and lower fault labeled F4 in McCalpin and Nelson, 2000) transected were underlain by normal faults with 7–9.5 m of vertical displacement measured on the top of Bonneville-age lake beds (ca. 15,500 years old).
>
> This soil argues for a long period of fault inactivity between ca. 7–8,000 years ago and 15,500 years ago. That time span is roughly 4 times as long as the typical intervals between major earthquakes on this segment of the WFZ. The quiescent interval

Fig. 10. Hidden Valley Park seismic line with author Sheley looking east. Flags represent geophone locations and the endpoint of the line is beyond the top of the scarp.

could be either an irregularity typical of the long-term behavior of the WFZ, or a response to the drying up of Lake Bonneville between 15,000 years ago and ca. 11,000 years ago, which relieved a huge weight on the down thrown fault block of the WFZ.

To validate and possibly extend the Megatrench results, University of Utah researchers in October, 1999 conducted a 2-D seismic survey across the same fault trace, but about 20 m north of the Megatrench. Fig. 4 shows the seismic line, which was about 15° sub-parallel to and located about 20 m north of the Megatrench. The seismic survey consisted of an 83.5-m line with 168 equi-spaced geophones, where each hammer position visited a geophone position. A typical shot gather is shown in Fig. 6 and Table 1 lists the field recording parameters.

Approximately, 27,000 first arrival times were picked from the shot records and inverted (see Table 2 for inversion parameters) to give the tomograms shown in Fig. 8. The final tomogram is shown in Fig. 8a, and shows three low-velocity zones that appear to be colluvial wedges. The LVZ A is interpreted as the colluvial wedge along the F4 fault in McCalpin and Nelson (2000), and LVZ B might be a deeper and older colluvial wedge that is somewhat larger than LVZ A. The deepest LVZ C might also be a colluvial wedge, but this interpretation is not convincing in light of the checkerboard test shown in Fig. 5.

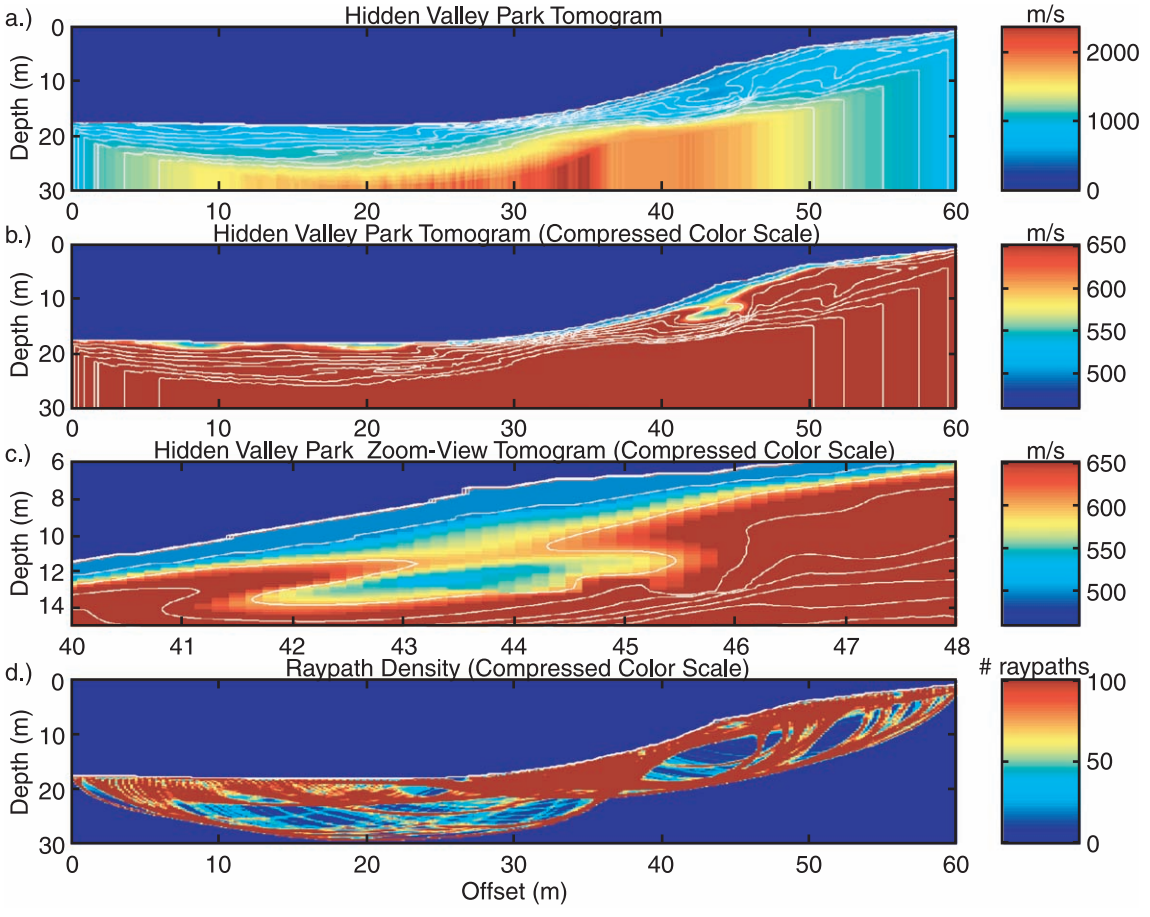

Fig. 11. Figures (a)–(c) depict different perspectives of the Hidden Valley Park tomogram, and (d) depicts the raypath density diagram. The raypath density provides a view of the regions that can be resolved by tomography.

The combination of the trench log, tomogram, and reflection migration image is given in Fig. 9. Here, the reflection section clearly reveals fault locations, while the tomograms provide secondary evidence for such faults. In the top illustration, a sketch of McCalpin and Nelson's trench log along the fault F4 is given along with our interpretation of the main and antithetic faults. These fault interpretations were mostly based on the seismic migration image shown at the bottom.

McCalpin (2002) suggest that the colluvial material in LVZ A resulted from displacement and filling that followed at least five large earthquakes that occurred in the following years: 1.3 KA, 2.4 KA, 3.9 KA, 5.3 KA, and 7.5 KA. McCalpin and Nelson (2000) report 15 KA Lake Bonneville sediment about 2 m below the bottom of LVZ A. Thus, LVZ B must be even older because it is 5–7 m below the bottom of LVZ A in the tomogram. LVZ B has a large thickness of about 4 m which may have been formed by a sequence of three or more large magnitude earthquakes, just like that for LVZ A. The physical separation of LVZs A and B suggests the possibility of two types of times scales for large events: a short-time scale of 6000 years or so where three or more events take place at F4 to form a large colluvial wedge package such as LVZ A. This is followed by a longer period of quiescence of 7000 years or more before activity resumes, such as the time interval between the last event for LVZ B and the earliest event for LVZ A. This is speculation until core samples are drilled and dated from LVZs B and C.

An LVZ in the tomogram alone does not provide unambiguous evidence of a colluvial wedge. Indeed, other geologic interpretations exist, such as a low-velocity sand wedge along the down thrown side of the fault. For this reason, we suggest conducting many parallel 2-D surveys across the fault. The consistent presence of similarly shaped LVZ's on the down-thrown side of the fault increases confidence in the colluvial wedge interpretation.

4.2. Hidden Valley Park results

Along the southern part of the Salt Lake segment is the Hidden Valley Park strand, located near 11500 South Wasatch Boulevard. This park is bisected by the southern end of the Salt Lake City segment of the Wasatch Fault, and is about six blocks south of the Dry Gulch (DG) site, and is about 4 km south of the Megatrench site. The parameters for the seismic experiment and inversion are listed in Tables 1 and 2, respectively, and a view of the site looking eastward is shown in Fig. 10.

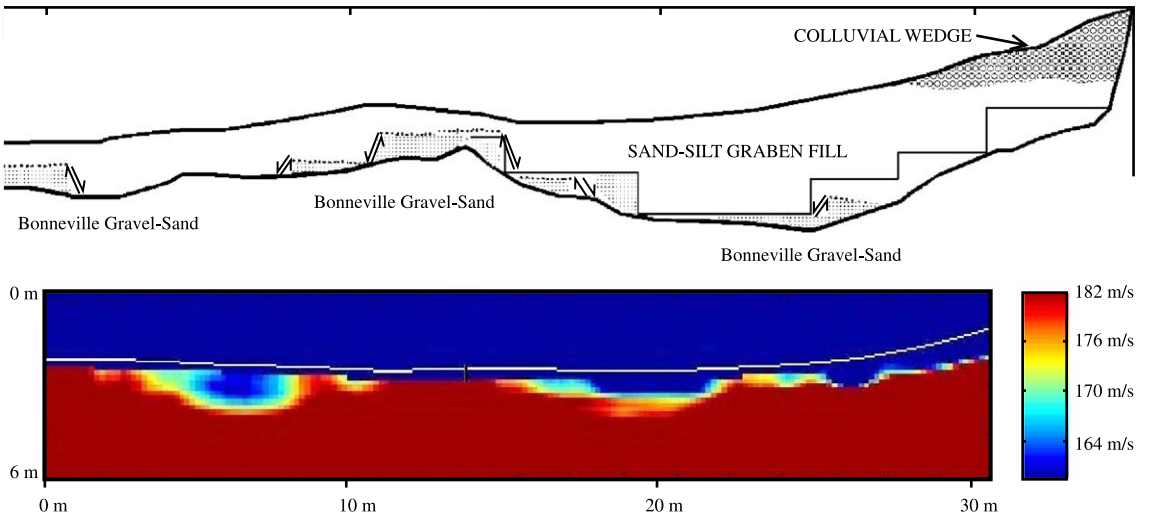

Fig. 12. (Top) Trench log redrawn from Delta Geotech. (1994) and (bottom) expanded view of the lower part of the tomogram from previous figure. Note the sharp features in the tomogram are consistent with faulted gravel beds in the trench log.

Fig. 11 shows the tomograms from inverting 8725 travel times. The lower part of the dark solid region defines the ground surface, and the tomogram at the offset of 45 m (Fig. 11c) is zoomed in and shown with a compressed color scale. It appears that there might be two LVZs in this zoom view, a disk-like LVZ that is at the surface and the wedge-like body centered at the depth of 13 m. These LVZs are likely related to the colluvial wedge (shown in Fig. 12 trench log) excavated about 50 m to the north by Delta Geotech. (1994).

There are several other LVZs in the tomogram, but they have resulted from geologic processes apart from colluvial wedge formation. Fig. 12 zooms in on these LVZs and also shows sketches from the nearby trench log. The trench log suggests that these LVZs are likely due to stream channels or faulted gravel beds.

4.3. Oquirrh fault result

The Oquirrh 2-D survey line is described in Morey and Schuster (1999).The 2-D data consisted of 384 shot gathers, where each shot gather contained 96 traces. The field experiment and inversion parameters are listed in Tables 1 and 2, respectively. Over 30,000 first-arrival travel times were picked from these data and inverted to give the tomograms shown in Fig. 13. Three LVZs are highlighted and shown with a com-

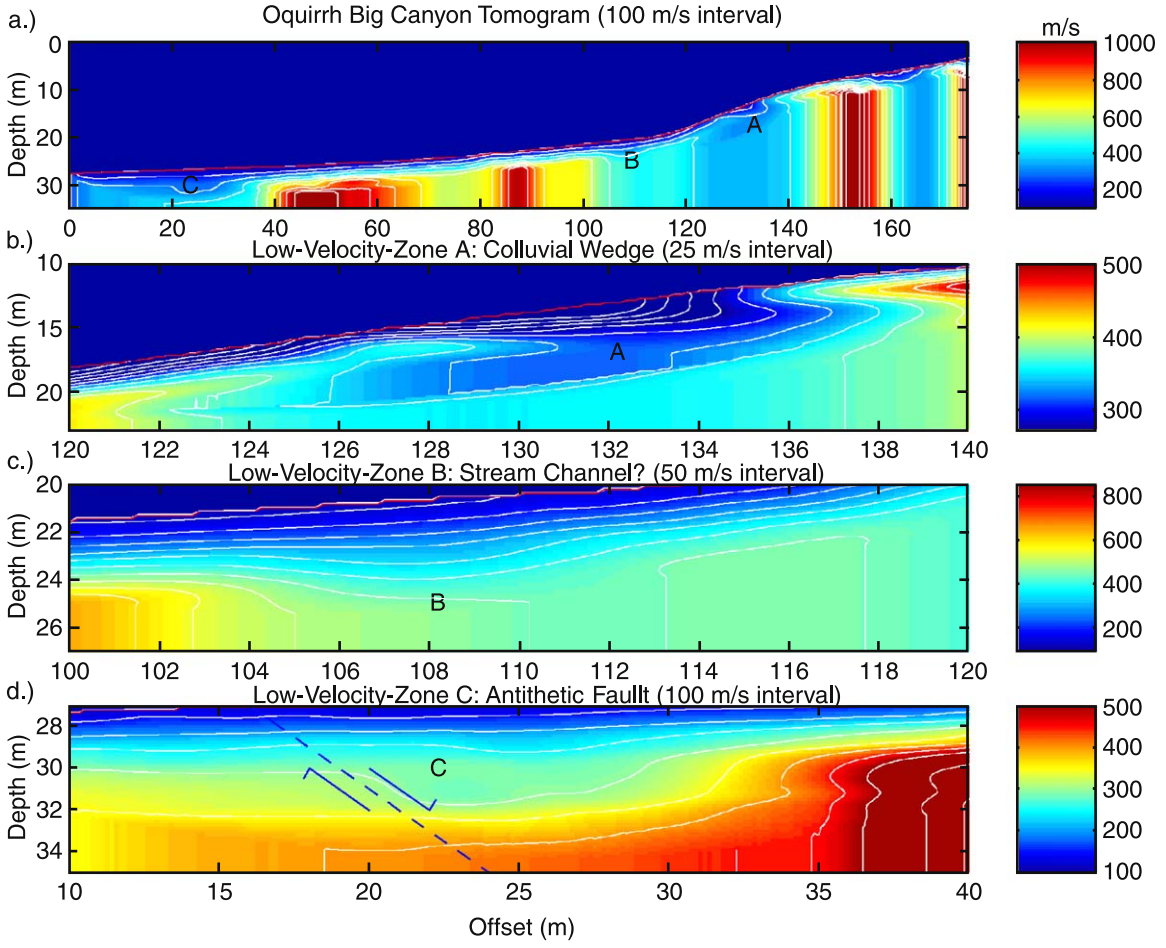

Fig. 13. Figure (a) depicts Oquirrh Big Canyon tomogram, and (b), (c), and (d) show zoom views of LVZs. LVZ A is the colluvial wedge shown in Morey and Schuster (1999), LVZ B is presumed to be the stream channel mentioned in Olig et al. (1996), and LVZ C is associated with the antithetic fault depicted in the next figure.

pressed color scale. The LVZ A roughly agrees in depth and thickness with the colluvial wedge shown in the trench log sketched in Morey and Schuster (1999) and obtained from Olig et al. (1996).There is also a good but not exact agreement with the 3-D tomogram image shown in Morey and Schuster (1999).

The LVZ B is not a colluvial wedge, but is likely a channel fill as suggested by the trench log in Olig et al. (1996).The bottom image in Fig. 13 shows a westward thickening of the low-velocity sediments and is in the location of the antithetic fault (Olig et al., 1996). Indeed, the reflection section shown at the bottom of Fig. 14 supports the presence of an antithetic fault at this location. Combining the tomogram and reflection migration section yields the final interpreted tomogram at the top of Fig. 14. As in the Megatrench survey, the reflection section reveals the bed truncations due to the fault, while the tomogram is best at detecting the colluvial wedge and interpreted stream channel.

As demonstrated in Morey and Schuster (1999), the thickness of a colluvial wedge combined with the far field layer tilt angle can be used to estimate the magnitude of an ancient earthquake. But now, this capability is possible with more practical 2-D surveys.

4.4. Judge memorial high school

The last survey took place in the middle of the football field at Judge Memorial High School, near

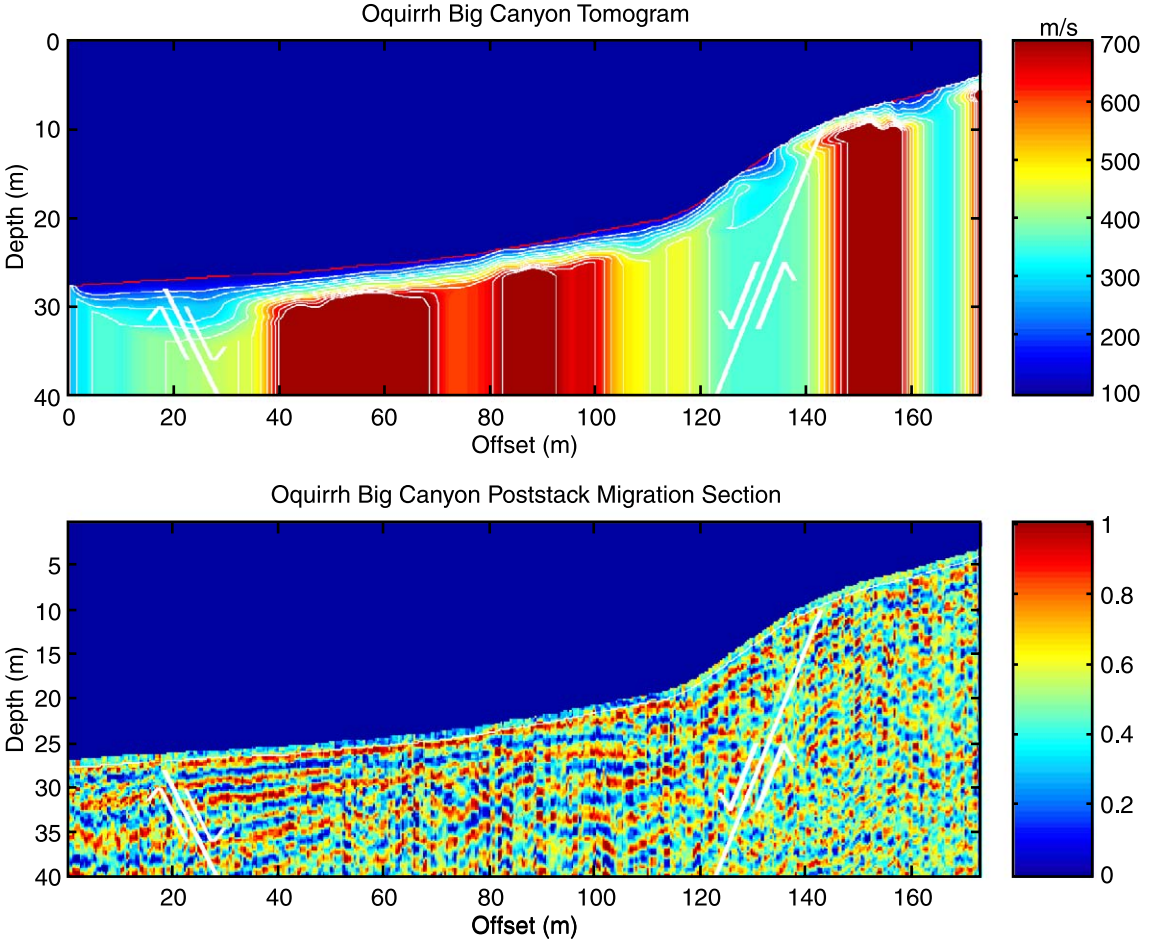

Fig. 14. (Top) Final interpreted Oquirrh tomogram and (bottom) migration reflection section. Antithetic fault is at left and main fault is at right.

the University of Utah. It was believed that a minor strand of the Wasatch fault cut across the football field and posed an earthquake hazard to school buildings. However, the evidence for this fault was somewhat tenuous, based on ambiguous ground-penetrating radar results. It was not known if a colluvial wedge characterized this fault.

In the spring of 2001, students at the Geology and Geophysics Department, University of Utah, carried out a shallow seismic survey. They collected a total of 120 shot gathers, with 120 traces per gather. Table 1 describes the parameters for the field experiment and Table 2 lists the inversion parameters. For the first time, GUI interactive processing software was used to process the reflection records.

Fig. 15 displays the (top) common offset gather, stacked reflection section (middle) and (bottom) three common midpoint gathers. Comparing the common midpoint gathers to the stacked section provides partial confidence that the stacked events identified as reflections are associated with reflections with hyperbolic moveout in the common midpoint gathers. The common offset gather is another means to convince us that events in the stacked section represent reflections seen in the common offset gathers.

Fig. 16 displays the tomogram, reflection section and migration section. In this case, the reflection section clearly reveals a fault at the location estimated by the ambiguous GPR survey. A colluvial wedge is not clearly identified in the tomogram nor is it obvious that there is a fault at the location suggested by the reflection section. This is possibly due to the fact that prior to the construction of the high school, the original land surface was leveled and the top 5–7 m of the football field now consist of artificial fill. This may have disturbed remnants of any pre-existing colluvial

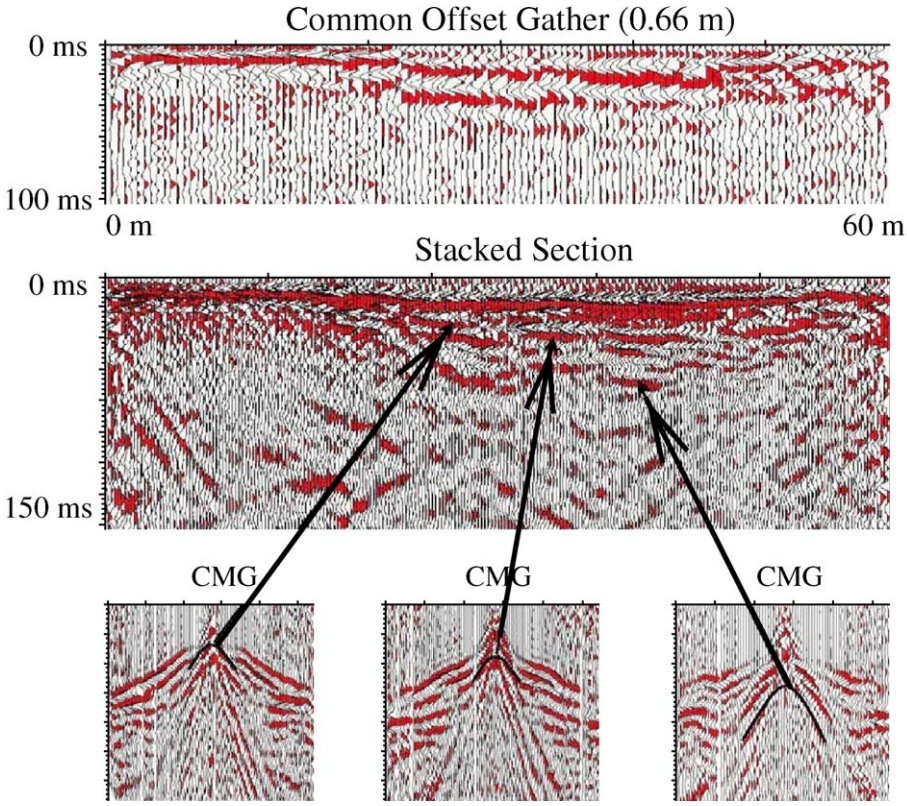

Fig. 15. (Top) Common offset gather, (middle) stacked reflection section and (bottom) common midpoint gathers from Judge High School experiment.

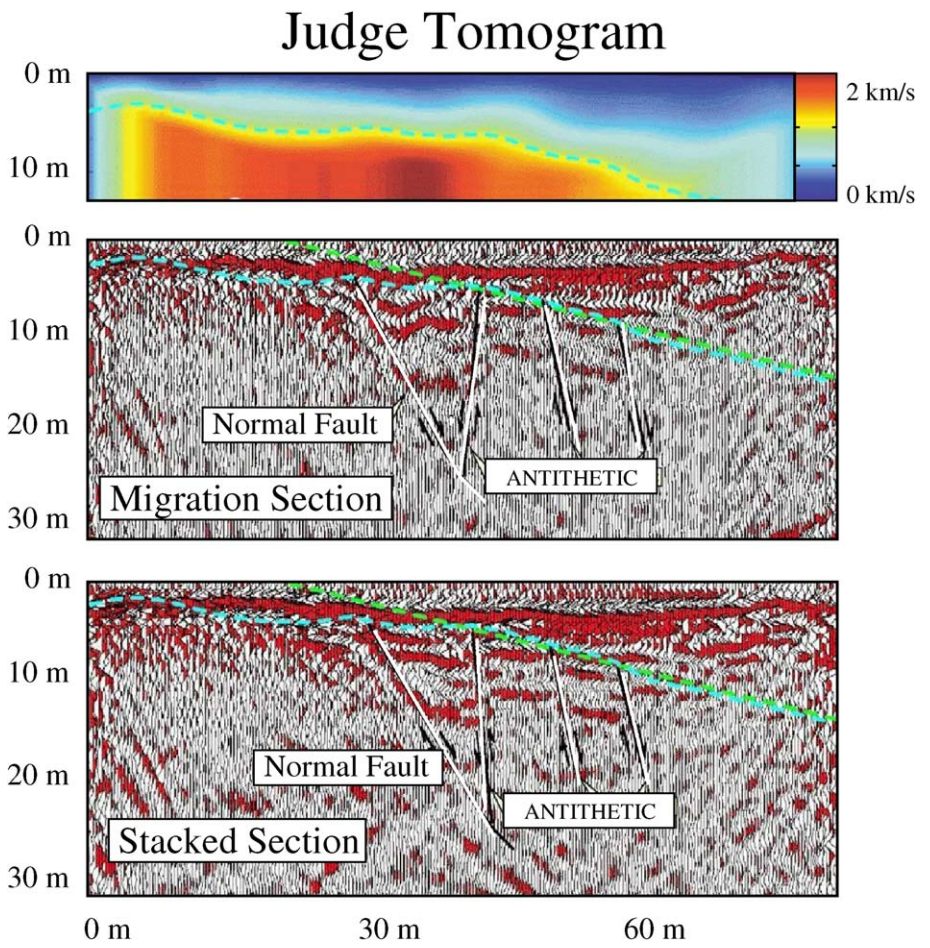

Fig. 16. (Top) Refraction tomogram, (middle) migration section and (bottom) stacked reflection section. Dashed line is contact between fill and original soil as estimated from reports and field observations.

wedges, and certainly truncated the fault before it reached the current surface of the football field.

The blue dashed line in the top two images in Fig. 16 corresponds to the estimated location of the fill bottom. This estimate was made by observing the depth of the fill at a road cut next to the football field, and projecting it to the survey line using the dip reported in original documentation from the field construction reports. Remarkably, the green dashed line and the boundary between the yellow and red tomogram velocities (denoted by the dashed blue line) are almost coincident (please refer to the online color figure). A lesson to be learned here is that interactive GUI based processing software can produce high quality reflection seismograms, and the tomograms can aid both in the processing and the interpretation.

5. Conclusions

Our results demonstrate that 2-D seismic trenching can delineate the shape and location of low-velocity zones, some of which are known to be colluvial wedges. It also suggests the possibility of imaging multiple colluvial wedges by seismic experiments to depths of 10 m or more. In the case of the Megatrench, the fault geometry is delineated by the reflection images and several LVZ's are interpreted as colluvial

wedges. It was surprising to discover that the large offset-to-depth ratio of 7 to 1 was needed to accurately image LVZs with a size of several meters.

An LVZ in a tomogram is most likely, but not certainly, a colluvial wedge if it is situated along the down thrown side of a normal fault, it is localized as an LVZ with the thickness and shape of a typical classic colluvial wedge, and it extends along the strike direction. Careful use of the color scale can also reveal features in the tomogram that are related to other geologic structures such as shallow graben faulting or stream channels. However, the tomogram cannot necessarily determine if a colluvial LVZ was formed by one very large event or by a sequence of smaller events as demonstrated by the Megatrench example. Thus, LVZs should be drilled, cored, and dated to unambiguously determine the history of the ancient earthquakes.

Although 2-D seismic surveys are much more practical than 3-D surveys, they will produce less certain results. The extra dimension along the fault strike in a 3-D tomogram can greatly reduce the uncertainty in identification of LVZs as wedges compared to a single 2-D survey. Thus, several 2-D profiles parallel to one another are recommended for greater certainty in interpretation. Our last survey at Judge High School suggested that careful processing of the reflection records can yield high quality imaging of the fault boundary. This was partly made possible by our increased experience in reflection processing and partly by using a reflection processing package with an interactive graphical user interface.

Overall, our results validate the use of inexpensive 2-D seismic trenching as a means to identify colluvial wedges to depths of 10 m or more. But the crucial step of age dating is not possible with seismic alone, so the next challenge is to drill through the identified wedges and date the cores. Drilling through cobbles is not a standard drilling procedure, but preliminary results appear to be promising in dating core samples from formations associated with seismically imaged colluvial wedges in the Great Salt Lake (Dinter et al., 2000). The successful identification of colluvial wedges by seismic trenching, their subsequent coring by drilling, and dating by radiocarbon analysis will allow palaeoseismologists to probe the past history of earthquakes deeper in earth and farther in time than ever before possible.

Acknowledgements

We thank Ron Bruhn for his valuable advice about palaeoseismology, and the following people for their assistance in the field experiments: M. Buddensiek, J. Sheng, F. Meng, Y. Wang, J. Chen, Z. Liu, G. Waite, E. Tartaras, H. Sun, D. Johnson, L. Xiang and, D. Lynch. We thank Doug Nelson and Ron Bruhn for their consultations on Wasatch fault geology, Colorado School of Mines for use of their SU processing software, and thanks to Sisimage for the use of their interactive seismic processing software Vista.

References

Aldridge, D.F., Oldenburg, D.W., 1993. Two-dimensional tomographic inversion with finite-difference traveltimes. Journal of Seismic Exploration 2, 257–274.

Ammon, C.J., Vidale, J.E., 1993. Tomography without rays. Seismological Society of America Bulletin 83, 509–528.

Black, B.D., Lund, W.R., Schwartz, D.P., Gill, H.E., Mayes, B.H., 1996. Paleoseismic investigation on the Salt Lake City segment of the Wasatch fault zone at the South Fork Dry Creek and Dry Gulch sites, Salt Lake County, Utah. Utah Geological Survey Special Study 92, 22.

Delta Geotechnical Consultants, 1994. Surface fault rupture and engineering geology investigation for the proposed Hidden Valley Park Subdivision, unpublished consultant's report submitted to Sandy City, Utah.

Dinter, D.A., Pechmann, J.C., Kelts, K., Schnurrenberger, D., Haskell, B., Valero-Garcs, B., Nielson, D., Palacios-Fest, M., Kruger, N., Cohen, A., Dean, W., 2000. Holocene palaeoseismology of the East Great Salt Lake fault: preliminary results of an integrated coring/high-resolution reflection seismic study of a submerged active normal fault. EOS, Transactions of the American Geophysical Union 81 (Supplement).

Gilluly, J., 1928. Basin and range faulting along the Oquirrh range, Utah. Geological Society of America Bulletin 39, 1103–1130.

Handwerger, D., Cerling, T.E., Bruhn, R.L., 1999. Cosmogenic 14C in carbonate rocks, preliminary results. Geomorphology 27, 13–24.

Lutter, D., Nowack, R., Braile, L., 1990. Seismic imaging of upper crustal structure using traveltimes from the PASSCAL Ouachita experiment. Journal of Geophysical Research 95, 4621–4631.

Matheney, M., Nowack, R., Trehu, A., 1997. Seismic attribute inversion for velocity and attenuation structure using data from the GLIMPCE Lake Superior experiment. Journal of Geophysical Research 102, 9949–9960.

Mattson, A., 2003. Temporal and Spatial Patterns of Normal Faults: Determined by Geomorphic, Geological, and Geophysical Techniques, Eastern Great Basin, Utah: PhD dissertation, University of Utah.

McCalpin, J.P., 1996. Paleoseismology. Academic Press, San Diego, CA, p. 588.

McCalpin, J.P., 2002. New age controls from the Wasatch Fault Megatrench 1999, GSA 54th Annual Meeting, Rocky Mountain Section.

McCalpin, J., Nelson, C., 2000. Long recurrence records from the Wasatch fault, Utah, USGS NEHRP Annual Report, Grant No. 99HQGR0058, p. 61.

McCalpin, J.P., Nishenko, S.P., 1996. Holocene palaeoseismicity, temporal clustering, and probabilities of future large (M>7) earthquakes on the Wasatch fault zone, Utah. Journal of Geophysical Research 101 (B2), 6233–6253.

Morey, D., 1997. Seismic CAT scan of an ancient earthquake along the Oquirrh fault, Utah, MS Thesis, University of Utah, Utah.

Morey, D., Schuster, G.T., 1999. Paleoseismicity of the Oquirrh fault, Utah from shallow seismic tomography. Geophysical Journal International 138, 25–35.

Nemeth, T., Normark, E., Qin, F., 1997. Dynamic smoothing in cross-well traveltime tomography. Geophysics 62, 168–176.

Nolet, G. (Ed.), 1987. Seismic Tomography: With Applications in Global Seismology and Exploration Geophysics. D. Reidel Publishing, Dordrecht, Holland, p. 386.

Olig, S.S., Lund, W.R., Black, B.D., Mayes, B.H., 1996. Paleoseismic investigation of the Oquirrh fault zone, Tooele County, Utah. Utah Geological Survey Special Study 88, 22–54.

Schuster, G.T., 1996. Resolution limits for crosswell migration and traveltime tomography. Geophysical Journal International, 427–440.

Schwartz, D.P., Coppersmith, K.J., 1984. Fault behavior and characteristic earthquakes—examples from the Wasatch and San Andreas fault zones. Journal of Geophysical Research 89 (B7), 5681–5698.

Sheng, J., Schuster, G., 2000. Finite-frequency resolution limits of traveltime tomography for smoothly varying velocity models. 70th Ann. Internat. Mtg., Soc. Expl. Geophys., Expanded Abstracts, pp. 2134–2137.

Smith, R.B., Arabasz, W.J., 1991. Seismicity of the intermountain seismic belt. In: Slemmons, D.B., Engdahl, E.R., Zoback, M.D., Blackwell, D.D. (Eds.), Neotectonics of North America. Geological Society of American Decade Map, vol. 1, pp. 185–228.

Stephenson, W.J., Smith, R.B., Pelton, J.R., 1993. A high resolution seismic reflection and gravity survey of quaternary deformation across the Wasatch fault, Utah. Journal of Geophysical Research 98 (B5), 8211–8223.

Williamson, P., Worthington, M., 1993. Resolution limits in ray tomography: numerical experiments. Geophysics 58, 727–736.

Wu, D., Bruhn, R.L., 1994. Geometry and kinematics of active normal faults, southern Oquirrh Mountains, Utah: implications for fault growth. Journal of Structural Geology 16, 1060–1075.

Yilmaz, O., 1987. Seismic Data Processing. Society of Exploration Geophysicists, Tulsa, OK.